Lipopolysaccharide O-antigen molecular and supramolecular modifications of plant root microbiota are pivotal for host recognition

Adele Vanacore,[a] Giuseppe Vitiello,[b] Alan Wanke,[c] Domenico Cavasso,[a] Luke A. Clifton,[d] Lisa Mahdi,[c] María Asunción Campanero-Rhodes,[e,f] Dolores Solís,[e,f] Manfred Wuhrer,[g] Simone Nicolardi,[g] Antonio Molinaro,[a] Roberta Marchetti,[a*] Alga Zuccaro,[c] Luigi Paduano,[a] Alba Silipo[a*]

[a] Department of Chemical Sciences and Task Force for Microbiome Studies, University of Naples Federico II, Via Cinthia 4, 80126, Naples, Italy
[b] Department of Chemical, Materials and Production Engineering, University of Naples Federico II, Piazzale Tecchio 80, 80125, Naples, Italy
[c] University of Cologne Cluster of Excellence on Plant Sciences (CEPLAS), Institute for Plant Sciences, D-50674 Cologne, Germany
[d] ISIS Pulsed Neutron and Muon Source, Science and Technology Facilities Council, Rutherford Appleton Laboratory, Harwell Science and Innovation Campus, Didcot, Oxfordshire OX11 OQX, UK
[e] Instituto de Química Física Rocasolano, CSIC, Serrano 119, 28006 Madrid, Spain
[f] CIBER de Enfermedades Respiratorias (CIBERES), Avda Monforte de Lemos 3-5, 28029, Madrid, Spain
[g] Prof. M. Wuhrer, Dr. S. Nicolardi, Center for Proteomics and Metabolomics, Leiden University Medical Center, Leiden 2333 ZA, The Netherlands

* Corresponding author. Email: roberta.marchetti@unina.it (RM); silipo@unina.it (AS)

Abstract

Lipopolysaccharides, the major outer membrane components of Gram-negative bacteria, are crucial actors of the host-microbial dialogue. They can contribute to the establishment of either symbiosis or bacterial virulence, depending on the bacterial lifestyle. Plant microbiota shows great complexity, promotes plant health and growth and assures protection from pathogens. How plants perceive LPS from plant-associated bacteria and discriminate between beneficial and pathogenic microbes is an open and urgent question. Here, we report on the structure, conformation, membrane properties and immune recognition of LPS isolated from the *Arabidopsis thaliana* root microbiota member *Herbaspirillum* sp. Root189. The LPS consists of an *O*-methylated and variously acetylated D-rhamnose containing polysaccharide with a rather hydrophobic surface. Plant immunology studies in *A. thaliana* demonstrate that the native acetylated O-antigen shields the LPS from immune recognition whereas the *O*-deacylated one does not. These findings highlight the role of *Herbaspirillum* LPS within plant-microbial crosstalk, and how O-antigen modifications influence membrane properties and modulate LPS host recognition .

1. Introduction

Plants provide a multitude of niches for the growth and proliferation of plant microbiota, a complex co-association of microorganisms comprising taxa from diverse phyla, including bacteria, fungi, protists and nematodes. Such a complex microbial community is persistent and ubiquitous, promotes plant health and growth, productivity and fitness, mediates beneficial transformation and mobilization of nutrients in the rhizosphere. Furthermore, plant microbiota increase host tolerance to biotic or abiotic stresses and prime immune responses and systemic resistance.(Trivedi, 2020; Delaux, 2021). The interaction is mutual, with the host plant providing unique metabolic capabilities to the associate microbial communities.

The cross-talk between plants and host microbiota represents a yet to be explored research field. The plant immune system perceives constitutive and conserved microbial epitopes, so-called microbe-associated molecular patterns (MAMPs), to elicit the first line of immune responses. This MAMP-triggered immunity controls the microbial load and, upon *non-self*-recognition, induces defense responses such as oxidative bursts, nitric oxide generation, extracellular pH increase, cell wall reinforcement, and accumulation of pathogenesis-related proteins to limit pathogen growth. MAMPs include proteins such as bacterial flagellin and elongation factor Tu as well as cell envelope components, like lipopolysaccharides (LPS) (Di Lorenzo, 2021; Wanke, 2021; Marchetti, 2021), beta-glucans (Wanke, 2020), peptidoglycan (Erbs, 2008), and fungal chitin (Hayafune, 2014).

Lipopolysaccharides, complex glycoconjugates indispensable for growth and viability of Gram-negative bacteria, represent the main constituent of the external layer of the outer membrane (Belin, 2018), that encases periplasm and peptidoglycan cell wall. LPSs are tripartite macromolecules built up of a glycolipid portion, the lipid A, linked to a glycan part consisting of a core oligosaccharide that mostly carries a polysaccharide portion, termed O-antigen (O-specific polysaccharide).

Plant growth-promoting rhizobacteria (PGPR) promote nitrogen fixation, phosphorus solubilization, phytohormones production, nutrient uptake and protect plants from disease and abiotic stress (Schlemper, 2018; De La Torre-Ruiz, 2016). Among PGPR, increasing interest in utilizing endophytic diazotrophs within the genera *Gluconacetobacter*, *Azoarcus*, *Azospirillum*, *Klebsiella*, *Serratia*, *Rhizobium* and *Herbaspirillum* is explained in their stable association with diverse, often economically relevant plant species, and their efficiency in nitrogen fixation. The Gram-negative genus *Herbaspirillum* belongs to the Betaproteobacteria class and comprises 14 species to date. *Herbaspirillum* sp. associates with model plants such as *Arabidopsis thaliana* (Bai, 2015) and economically important crops in the family Poaceae and increase growth and productivity (Monteiro, 2012). The initial colonization steps are mediated by bacterial envelope components, such as lipopolysaccharide, exopolysaccharide and adhesins and by the type three secretion system, whose expression can be modulated following recognition of plant signals. In fact, *H. seropedicae* LPS is

required for plant colonization, as mutant strains impaired in LPS biosynthesis showed a severe reduction in attachment to the maize root surface and affected internal maize tissue (Balsanelli, 2012; Tadra-Sfeir, 2011).

Evasion or suppression of the plant immune recognition is therefore not only essential for pathogens to successfully infect plant hosts but must be also critical for commensals to colonize different plant niches or establish successful symbiosis. How plant innate immune system discriminates between beneficial and pathogenic microbes, and *vice versa,* how beneficial microbes evade plant perception remains largely unknown (Hacquard, 2017), especially from the molecular point of view. Within this scenario, different studies provided evidence for receptor competition that allows (rice) plants to discriminate microbial cell wall signals and balance immunity and symbiosis signaling (Zhang, 2021). However, it is not clear if the microbe itself can work to adjuvate the process. To this end, we sought a molecular level dissection of structure and function of the LPS from the root microbiota member *Herbaspirillum* sp. Root189, isolated from the roots of *Arabidopsis thaliana* (Wanke, 2021; De La Torre-Ruiz, 2016). By this work, we could i) define and correlate the structure of *Herbaspirillum* LPS to the properties of its cell envelope; ii) dissect the chemical features at the basis of host-microbe crosstalk, iii) identify the glycan modifications that tune the appropriate interaction with host immune receptors.

2. Material and Methods

2.1 *Herbaspirillum* LPS extraction, purification and compositional analysis

Dried *Herbaspirillum* cells were extracted with the hot phenol/water procedure (Westphal & Jann, 1965), purified via enzymatic treatments and size exclusion chromatography and analysed via SDS-PAGE. The sugar composition was established using acetylated alditols and acetylated O-methyl glycosides methods (De Castro, Parrilli, Holst & Molinaro, 2010). Linkage analysis was performed using Ciucanu-Kerek's method (Ciucanu & Kerek, 1984). Total fatty acid content was characterized as fatty acid methyl esters. Experimental details can be found in the supporting information.

2.2 Isolation of O-antigen polysaccharide and NMR spectroscopy

A mild acid hydrolysis with acetate buffer (pH 4.4) for 5 h at 100 °C was performed on the LPS in order to split the Lipid A and the OPS portions. The glycolipid part was separated from the hydrophilic carbohydrate part using Blight-Dyer's method (Bligh & Dyer, 1959). NMR spectra were recorded in D_2O at 298 K on a Bruker 600 AVANCE NEO equipped with a cryoprobe. For structural assignments of isolated OPS. Further details are given in the supporting section. Homonuclear and heteronuclear NMR experiments were permed as detailed in supporting information.

2.4 Mass spectrometry

Ultrahigh-resolution MALDI mass spectrometry (MS) analysis was performed on a 15 T solariX XR Fourier transform ion cyclotron resonance (FT-ICR) (Bruker Daltonics) system and 1 µL of de-acetylated OPS was spotted onto a "ground steel" 384 MALDI target plate (Buker Daltonics) with 1 µL of 1 mM sodium chloride and

1 µL of 10 mg/mL "super-2,5-dihydroxybenzoic acid (DHB)" [a 9:1 (w/w) mixture of DHB and 2-hydroxy-5-methoxybenzoic acid], in acetonitrile/water 50:50 (v/v) (Nicolardi, 2021). Each mass spectrum, generated from 200 laser shots with laser power at 30%, was acquired in the *m/z*-range 3493-30000 with 512 K data points (transient time 3.985 s). Further details are given in the supporting section.

2.5 Microarray Binding Assays

Herbaspirillum Root189 LPS was printed as triplicates at six different concentrations (from 1 to 0.003 mg ml^{-1}) on 16-pad nitrocellulose-coated glass slides (Grace Biolabs ONCYTE NOVA) using a non-contact arrayer (Sprint, Arrayjet Ltd.) (Campanero-Rhodes, 2021). Control (glyco)proteins (fetuin, asialofetuin, ribonuclease B, and ribonuclease A) were printed in parallel at concentrations ranging from 1 to 0.03 mg ml^{-1}. 1 µg ml^{-1} of Cy3 fluorophore (GE Healthcare) was added to the LPS and (glyco)protein solutions to enable post-array monitoring of the spots (Campanero-Rhodes, 2006) by scanning fluorescence signals upon excitation at 532 nm (green laser), using a GenePix 200-AL scanner (Axon, Molecular Devices). For binding assays, the microarrays were first blocked for 1 h with 0.25% (v/v) Tween-20 in 5 mM sodium phosphate, pH 7.2, 0.2 M NaCl (PBS) or in 10 mM Tris pH 8, 150 mM NaCl (TBS). Then, the arrays were overlaid for 1.5 h with biotin-labelled lectins at 10 µg ml^{-1} in an appropriate buffer containing 0.1% (v/v) Tween-20. A panel of 35 lectins was tested (see Table S1 for details on lectins tested, source, and buffer used in each case). Lectin binding was detected by incubating with AlexaFluor-647 (AF647)-labelled streptavidin (Invitrogen) at 1 µg ml^{-1} in PBS or TBS, 0.1% (v/v) Tween-20, for 35 min in the dark. The slides were scanned for AF647 signals (excitation at 635 nm, red laser) using a GenePix 200-AL scanner. Further details are given in the supporting section.

2.6 Plant material and growth

For the immune response assays, *Arabidopsis thaliana* Col-0 lines expressing cytoplasmic apoaequorin (Col-0_{AEQ}) were used (Knight et al., 1991). Seeds were surface, dried and sown onto ½ Murashige & Skoog (MS) medium (pH 5.7) supplemented with 0.5% sucrose and 0.4% Gelrite (Duchefa, Haarlem, the Netherlands). After stratification (3 days at 4°C), seeds were germinated for 7 days in climate chambers with an 8/16 h light/dark regime (light intensity of 110 µmol m^{-1} sec^{-1}) at 22/18°C. For oxidative burst assays, seedlings were transplanted into soil and grown for further three weeks. For calcium influx assays, seedlings were transferred into liquid ½ MS medium and grown for five more days.

Elicitor preparation All LPS preparations were solved at a concentration of 1 mg ml^{-1} and incubated on a rotary shaker for 4 hours prior to use in the immunity assays. Final elicitor concentrations applied in the assays were 250 nM flg22 (GenScript, Piscataway, USA) and 200 µg ml^{-1} of the LPS preparations for both complete LPS and its substructures. *Oxidative burst assay* Measurement of elicitor-triggered ROS production was performed as previously described (Wanke et al., 2020). In brief, leaf discs (3 mm) from 28 days-old *A. thaliana* Col-0_{AEQ} plants were incubated in white 96-well plates containing 200 µl MilliQ-water overnight at room temperature. Next day, the water was exchanged by 100 µl of fresh MilliQ-water containing 20 µg ml^{-1} horseradish peroxidase (Sigma- Aldrich, Taufkirchen, Germany) and 20 µm L- 012 (Wako Chemicals, Neuss, Germany). Plates were incubated for 20 minutes in the dark. Then, 100 µl of double-concentrated elicitor solutions were added. Chemiluminescence measurements were started immediately after elicitor addition using a TECAN SPARK 10M multimode microplate reader (constant measurement, 450 msec integration time). *Calcium influx assay A.*

thaliana Col-0_{AEQ} seedlings (12-days-old) were transferred into white 96-well plates containing 200 µl MilliQ-water. Just before overnight incubation in dark, water was replaced by 150 µl of 10 µM coelenterazine (Roth, Karlsruhe, Germany) diluted in MilliQ-water. Next day, 96-well plates were placed into TECAN SPARK 10M microplate reader for chemiluminescence measurement (constant measurement, 450 msec integration time). After baseline measurement (5 min), 50 µl of fourfold-concentrated elicitor solution was added to the wells. Main measurement was performed for 30 min, followed by discharge of remaining aequorin using 100 µl discharge buffer (30% EtOH, 3 M $CaCl_2$). Measured chemiluminescence values (in relative light units) of each well were normalized to the corresponding total detected chemiluminescence.

2.7 Static and Dynamic Light Scattering (SLS and DLS) characterization.

SLS and DLS measurements were performed at a concentration of 1 mg·mL^{-1}, at 25 °C and angle θ = 90°, by using a home-made instrument composed by a Photocor compact goniometer, a SMD 6000 Laser Quantum 50 mW light source operating at 532.5 nm, a photomultiplier (PMT120-OP/B) and a correlator (Flex02-01D) from Correlator.com. (Vaccaro, 2007) Since the size of Root189 LPS is less then λ/10, the only dependence from the concentration was studied. The mass-average molecular weight M_w and the second virial coefficient B of each polysaccharide were determined by means of Zimm plot analysis $\frac{Kc}{R_\theta} = \frac{1}{M_w} + 2B$ (1). In DLS, the correlation function was analyzed with a modified version of CONTIN. At least 5 independent measurements for each sample were analyzed with "Precision Deconvolve", a program based on the approach of Benedek and Lomakin (Lomakin, 2005). The proper diffusion coefficients were determined through a final assessment by the "regularization" procedure (Vitiello, 2015). Diffusion coefficients were then employed to calculate hydrodynamic radii by means of Stokes-Einstein relation (2).

2.8 Supported *Herbaspirillum* LPS containing bilayers deposition and Neutron Reflectivity

Herbaspirillum LPS-containing bilayers was deposited on the surface of single silicon crystals using a purpose-built Langmuir-Blodgett (LB) trough (KSV-Nima, Biolin Scientific, Finland), LB deposition was used to create the inner leaflet of the membrane on the support, and Langmuir-Schaeffer (LS) deposition was used to realize the outer leaflet. Details on the asymmetric bilayer preparation are given in the supporting section. Specular neutron reflectometry (NR) measurements were carried out using the white beam INTER reflectometer at the Rutherford Appleton Laboratory (Oxfordshire, UK), using neutron wavelengths from 1 to 16 Å. The reflected intensity was measured at two glancing angles of 0.7° and 2.3° as a function of the momentum transfer, Qz =(4πsinθ)/λ, where λ is wavelength and θ is the incident angle]. Neutron and X-ray reflectivity data were analyzed using the in-house software, RasCal (version 1, A. Hughes, ISIS Spallation Neutron Source, Rutherford Appleton Laboratory), which employs an optical matrix formalism to fit Abeles layer models to the interfacial structure. In this approach the interface is described as a series of slabs, each of which is characterized by its scattering length density (SLD), thickness, and roughness. The reflectivity for the model starting point is then calculated and compared with theexperimental data. A least-squares minimization is used to adjust the fit parameters to reduce the differences between the model reflectivity and the data. Further details in the supporting section.

2.9 MM and MD simulation.

Molecular mechanics calculations were performed with the AMBER* forcefield as included in MacroModel 8.0. A dielectric constant of 80 was used. For each disaccharide structure, both Φ and Ψ were varied incrementally

with use of a grid step of 18°, each (Φ,Ψ) point of the map being optimized with 2000 P.R. conjugate gradients. MD simulations were carried out using AMBER 18 suite of programs. Atom types and charges were assigned according to AMBER GLYCAM-06j-1 force field. By using the Leap module, the ligands were hydrated with octahedral boxes containing explicit TIP3P water molecules 10 Å away from any atom, also, counter ions were added to neutralize the system. The systems minimization was performed using Sander and MD simulations were carried out using the CUDA, which are distributed within the AMBER 18 package. The SHAKE algorithm was applied to all hydrogen containing bonds, and a 2 fs integration step was used. Periodic boundaries along with particle-mesh Ewald summation were used to compute long-range electrostatic interactions. Simulation was performed under isothermal and isobaric conditions. Trajectory coordinates were sampled every ps in order to acquire 10000 structures of the progression of the dynamics. Trajectories were visualized with VMD molecular visualization program.(Roe & Cheatham, 2013) and analysed with the ptraj module included in the AMBER18; data were visualized with SigmaPlot software (Systat Software, San Jose, CA). Further details in the supporting section.

3. Results and Discussion

3.1 *Herbaspirillum* Root189 LPS structure, conformation and membrane properties.

Herbaspirillum Root189 cells were extracted using the hot phenol-water procedure, LPS was found in the phenol phase and further purified by enzymatic treatments and gel filtration chromatography. The compositional analysis revealed the occurrence of D-rhamnose (Rha), 3-*O*-methyl-D-rhamnose (Rha3OMe), and as minor (likely core region) constituents, of D-glucosamine (GlcN), 3-deoxy-D-*manno*-oct-2-ulosonic acid (Kdo), L-*glycero*-D-manno-heptose (L,D-Hep), D-glucose (Glc) and 4-amino-L-arabinose (Ara4N). In addition, as acyl moieties, 10:0 (3-OH), 12:0 (3-OH) and 16:0 were found. Methylation analysis revealed the presence of 2,3-disubstituted Rha*p*, 3-substituted Rha*p*, and 4-substituted Rha*p*.

OPS structure. To isolate *Root189 O*$^-$ specific polysaccharide chain (OPS), an aliquot of LPS was cleaved by mild acid hydrolysis to split the lipid A moiety from the OPS, that afterward underwent extensive NMR investigation. The anomeric configuration of the monosaccharide units was assigned based on $^3J_{H1,H2}$ and $^1J_{C1,H1}$ coupling constants and confirmed by *intra*-residual NOE contacts; vicinal $^3J_{H,H}$ coupling constants and *intra* residual NOE contacts revealed the relative configuration of the sugar residues. Four spin systems were identified **A**, **B, C** and **D** (Figures 1A-B and S1, Table S1). Residues **B** and **C** were identified as α-rhamnose units, as attested by the scalar correlations of the ring protons with the methyl signal at position 6, visible in the TOCSY spectrum. The *manno* configuration was established by $^3J_{H-1,H-2}$ and $^3J_{H-2,H-3}$, both below 2 Hz, and diagnostic of the H-2 equatorial orientation; the α-anomeric configuration was assigned by the $^1J_{CH}$ coupling constant value (above 175 Hz). Spin system **A** was analogously identified as a 3-*O*-methyl-α-rhamnose; the 3-*O*-methyl group was

univocally located by the downfield shift of C-3 **A** (Table S2), its long-range correlation with the proton signals of methoxy group in the HMBC spectrum (Figure 1C) and confirmed by the NOE contact of this latter with H-3 **A** (Figures 1B-C and S1). Residue **D** was identified as a β-rhamnose, the anomeric configuration based on the $^{1}J_{CH}$ coupling constant value (162.0 Hz) and confirmed by the *intra*-residual NOE correlations between H-1 and H-3 and H-5. Furthermore, the down-field shift of H-2 proton resonance and its long-range correlation with the carbonyl carbon of an acetyl group, were all diagnostic of *O*-acetylation at this position. Minor OPS variants were also identified, differing for the acetylation pattern of the OPS repeating unit: a deacetylated OPS glycan chain as well as other species with further non-stoichiometric acetylation degree, *i.e.*, at O-3 of **B** and O-2 of **C** (respectively red and grey colored in table S2).

The downfield shift of carbon resonances identified the glycosylated positions: O-2 of **A**, O-4 of **B,** O-3 of **C** and O-3 of **D**. The *inter*-residual NOE contacts together with the long-range correlations derived from the HMBC spectrum (Figures 1B and S1), between **A**1 and **D**3; **D**1 and **B**4, **B**1 and **C3**; **C**1 and **A**2 described the O-antigen repeating unit of *Herbaspirillum* Root189 LPS depicted in Figure 1B and 2. The acetyl groups on **B** and **C** are nearly stoichiometric (< 30%) whereas the acetylation on **D** is above 70%. Of note, the complex and heterogeneous nature of the long saccharide chain of *Herbaspirillum* Root189 was also evident from the ^{1}H NMR on the intact LPS (Figure 1A), comparable to the isolated OPS as also the related HSQC spectrum (not shown).

OPS-deO. Further, an *O*-deacylation of *Herbaspirillum* O-antigen was performed to simplify the saccharide skeleton; the corresponding NMR spectra were thoroughly studied (Table S2, Figures 1A and S2). The four above rhamnose residues were identified, the anomeric configuration and sugar sequence were confirmed. In addition, an aliquot of *Herbaspirillum* OPS-de*O* was analyzed by ultrahigh-resolution MALDI FT-ICR MS (Figures 1C and S3) (Nicolardi, 2021). The OPS resulted oligodisperse with three major species detected. The additional heterogeneity observed in the mass spectrum may be the result of in-source fragmentation processes and/or heterogeneous sodium addition. The observed *m/z* difference between the three major ion species well matched the theoretical mass of 599.255 Da of the fully deacylated repeating unit (Figure 1C); this leads to an estimation of 13 to 15 tetrasaccharide repeating units taking also into account the presence of the core oligosaccharide region in the LPS. Both the OPS (Figure 2) and its de-acylated derivative were used to evaluate the immune perception by host plants (see below).

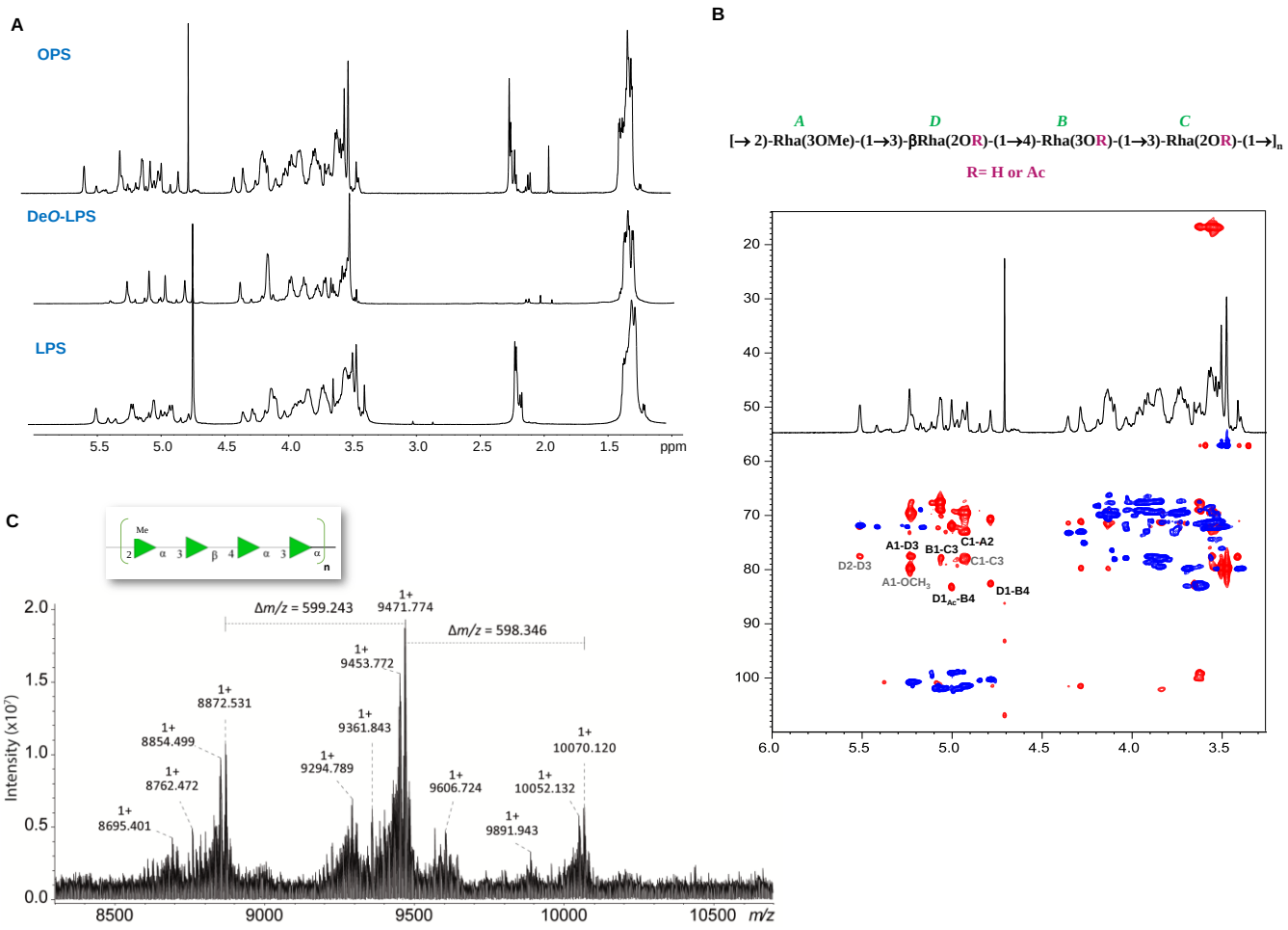

Figure 1. (**A**) Comparison of ^{1}H NMR spectra of *Herbaspirillum* LPS, OPS and O-deacylated LPS. (**B**) HSQC (blue) and HMBC (red) NMR spectra of *Herbaspirillum* OPS; the key *inter*-residual correlations were indicated; letters are as in table S1. Unless specified, Rhamnose residues are α-configured. (**C**) MALDI FT-ICR mass spectrum of de-acetylated OPS.

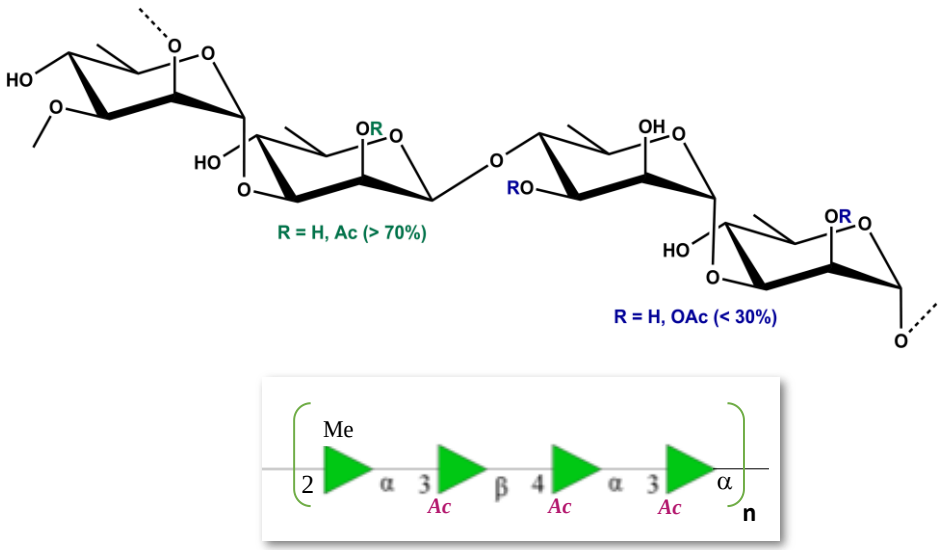

Figure 2. *Herbaspirillum* Root189 LPS O-antigen structure.

3.2 OPS conformational features.

The conformational behavior of *Herbaspirillum* Root189 OPS and OPS-de*O* was investigated by molecular mechanics and dynamic simulations. The potential energy surfaces of the four disaccharides constituting OPS repeating unit were constructed to evaluate the energetically accessible conformational regions. The corresponding adiabatic energy maps for the glycosidic torsions Φ (H1-C1-O-CX') and Ψ (C1-O-CX'-HX') are reported in Figure S4. For each disaccharide, the global minimum values were in accordance with the *exo*-anomeric effect. The energy maps showed moderate flexibility around Φ torsion and higher flexibility around Ψ angle, particularly for the Rha→3Rha, Rha(3OMe)→3βRha and Rha→2Rha(3OMe) disaccharide units, characterized by two global minima separated by a low energy barrier and corresponding to exo-Φ/syn-Ψ conformations (Figure S4). The lowest energy region of βRha→4Rha glycosidic linkage was centered around Φ/Ψ 60°/0°, however, the disaccharide also experienced a minimum in the exo-Φ/anti-Ψ conformation (Figure S4).

Using Φ and Ψ values obtained by MM calculation, saccharide structures encompassing respectively one and two repeating units of OPS-de*O* were constructed and the available conformational space was next investigated by MD simulations. The corresponding Φ/Ψ scatter plots, displayed in Figure S4B, confirmed the conformational regions energetically accessible to the disaccharide units and the preference for the *exo*-anomeric conformation around all the glycosidic linkages. This resulted in a limited flexibility and a relatively extended conformation of the glycan chain of *Herbaspirillum O*-deacetylated OPS (Figure S5-S6, table S2).

MD simulation was then employed to explore the conformational space available to the main acetylated *Herbaspirillum* OPS. Hexa- and deca-saccharides computational models, encompassing one and two repeating units, were constructed and subjected to MD simulations (Figures 3 and S4-S5). The initial structures were extensively minimized and subjected to an MD simulation of 100 ns in explicit water with AMBER18. For all the MD simulations, ensemble average interproton distances were extracted and translated into NOE contacts according to a full-matrix relaxation approach. Notably, the average distances obtained for the MD simulation from $\langle r^{-6} \rangle$ values were compared to those collected experimentally, and an excellent accordance between the experimental and calculated data was found (Table S2). Interestingly, the hydrophobic substituents on the glycan chain influenced shape and hydrophobicity of *Herbaspirillum Root189* OPS. Actually, the *O*-acetyl groups substituting the OPS induced slightly changes to the potential energy surface of βRha→4Rha disaccharide units, affecting the orientation of the glycosidic linkage that therefore included a further conformation characterized by Ψ values of 180°, corresponding to the *exo*-anti orientation around the glycoside torsion angle (Figures 3A). Therefore, compared to OPS-de*O*, the acetyl group substitution contributed to tune the overall conformation and properties of the saccharide chain, characterized by a higher degree of flexibility and a slight reduction of the extensions of the shape, described by a loose coiled-like structure (Figures 3B-

C, and figures S5-S6). The superimposition of the most representative conformations clearly shows that the acetyl and methyl groups protrude from the same face of the polymer backbone (Figure 3B-C). Accordingly, the acetyl groups of the polysaccharide chain cause an increase of hydrophobicity prevalently on one side of the polymer (Figure 3).

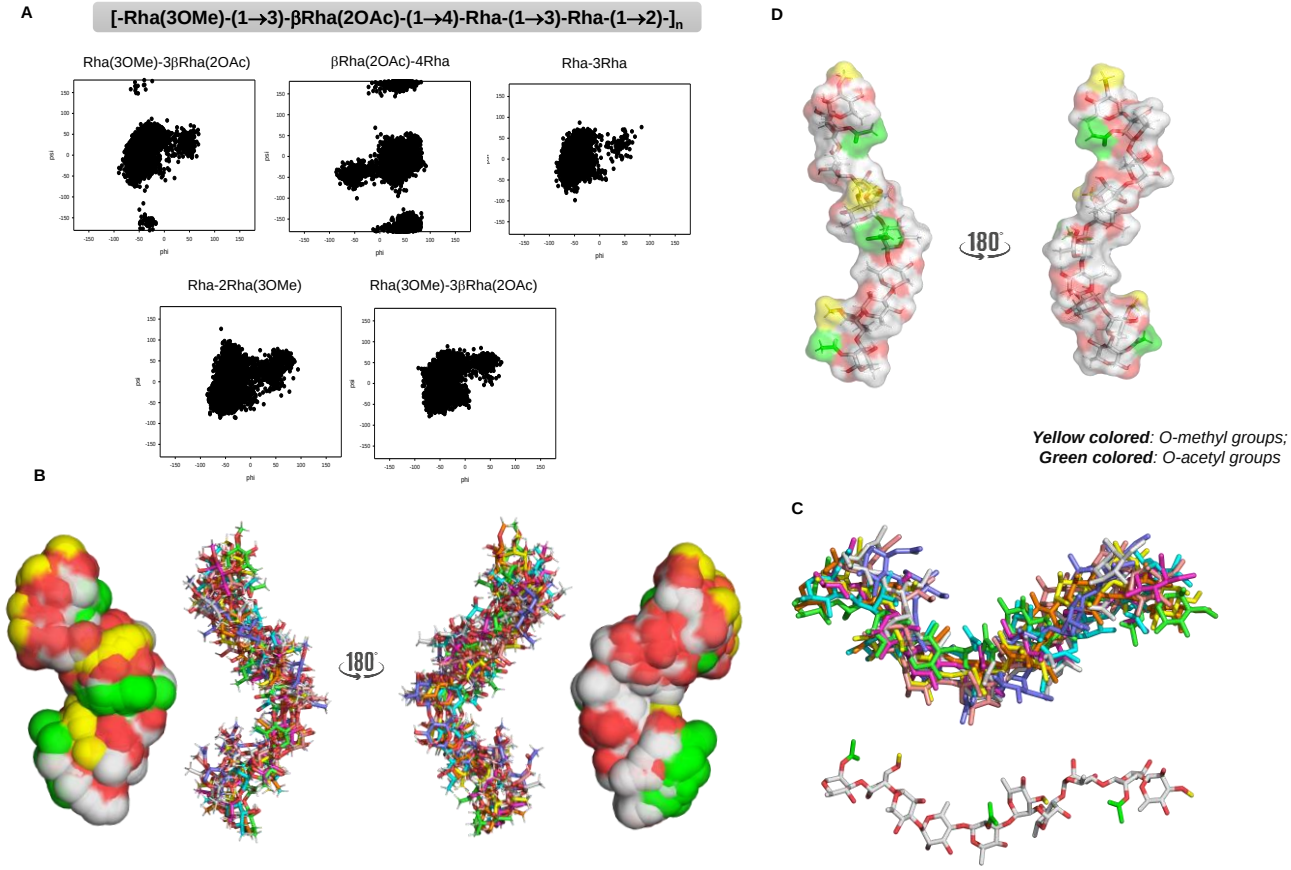

Figure 3. (A) scatter plots of Φ *vs.* Ψ along the MD simulation for the disaccharide units contained in *Herbaspirillum* Root189 OPS. **(B-C)** *Herbaspirillum* OPS conformational behaviour: Representative decasaccharide conformers and molecular surfaces of *Herbaspirillum* Root189 OPS as obtained by NMR and molecular dynamic simulation. The distribution of the *O*-Methyl and *O*-acetyl groups is highlighted with a color code (specified on the figure). Interestingly, for all the represented conformers only one side of the glycan chain is occupied by the non-sugar substituents. In **(D)** a representative conformation is chosen to show the coiled-like conformation of *Herbaspirillum* Root189 LPS O-antigen.

3.3 Solvent affinity, hydration and supramolecular properties of Root189 bilayers: Light scattering and Neutron reflectometry (NR) measurements.

Size of the LPS-forming aggregates as well as molecular mass and number of molecules involved in self-aggregation were determined by dynamic and static light scattering (DLS/SLS) measurements. (Vitiello, 2021) DLS measurements revealed a single LPS distribution centered at a hydrodynamic radius of 21.0 ± 1.0 nm (Figure 4A and supporting information). Each aggregate was constituted by around 35 LPS molecules, according to the average polymer molecular weight determined by MS. The hydrodynamic radius was in good agreement with the NR measurements obtained in the lipid bilayer (describe below). Furthermore, the value of the second virial coefficient was determined from the slope

of the Zimm plot in order to evaluate the solvent affinity to the LPS molecules; its positive value ($(1.9\pm0.1)\times10^{-4}$ mol·ml·g^{-2}) suggested a good hydration of the LPS bilayer (Figure 4A) (Perfetti, 2020). NR measurements were performed on an asymmetric bilayer composed of perdeuterated DPPC (inner leaflet)/*Herbaspirillum*-LPS (outer leaflet) deposited on silicon surfaces. NR is a powerful technique to reveal intricate molecular details of lipid bilayers, furnishing punctual information on the microstructural organization at nanoscale level of LPS-containing biomembranes. Three solution contrasts were used to get different reflectivity profiles of the asymmetric bilayer, constrained to fit a single profile of layer thickness and roughness. The hydration/volume fraction of the silicon deposited bilayer was evaluated by varying the data fits from each isotopic contrast in the Scattering Length Density (SLD) of each individual layer. Therefore, the structure of the lipid bilayer as well as surface coverage and interfacial roughness were evaluated by both parameter fit values and scattering length density profiles. NR results (Figure 4B) highlighted how a highly asymmetric lipid bilayer was placed at the silicon water interface, with the inner leaflet mainly composed of DPPC and the outer layer composed of *Herbaspirillum* LPS, as derived by the values of parameters obtained by NR fits (Table S3). In agreement, phosphocholine groups of DPPC constituted the inner headgroup region whereas the outer leaflet was built up by carbohydrate moiety of the LPS. The hydrophobic tails region was about 25 Å thick, contained only about 15% hydration, and the whole lipid bilayer was about 6 Å rough. This inner headgroup layer, about 5±1 Å thick, contained 85% hydration, mostly likely ascribable to water molecules associated with the hydrophilic phospholipids headgroups, suggesting a great amount of penetrating water molecules. The outer headgroup region of the bilayer was significantly thick, with a ~30 Å thick core region protruding outwards. The *O*-polysaccharide region occupied around 100Å in thickness, consistent with a significant molecular extension of the OPS coat, and was ~45Å rough, thus suggesting a large spacing between the OPS molecules in the lipid bilayer. Furthermore, a significant water penetration, with the OPS layer found to contain up to 87% hydration, characterized *Herbaspirillum* asymmetric bilayer.

Therefore, the structure and substitution pattern of the LPS *O*-antigen affects glycan chain extension and shape, the wide and bulky arrangement of the OPS regulate hydration and packing of the reconstituted bacterial outer membrane.

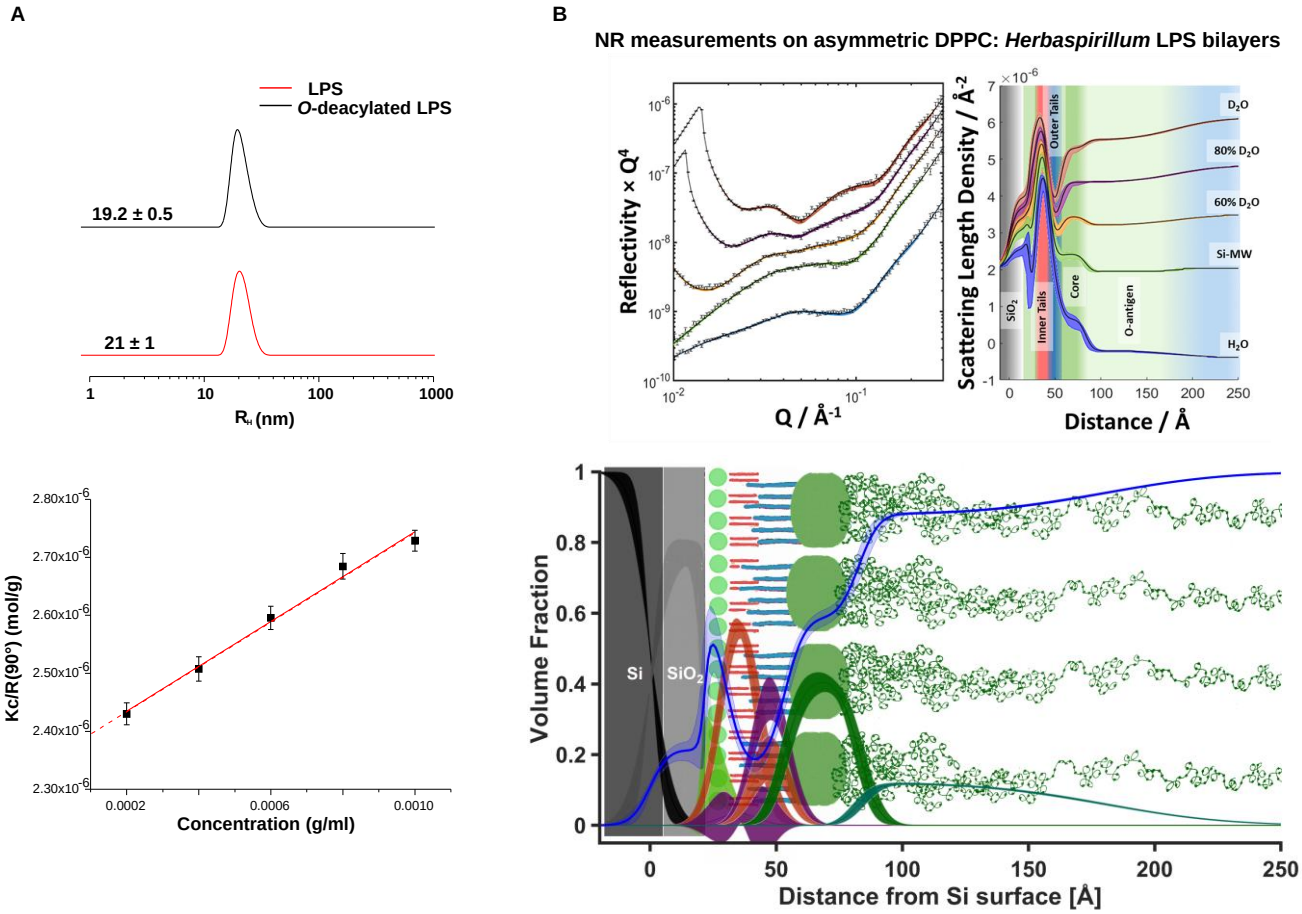

Figure 4. (A) Hydrodynamic radius and Zimm plot of *Herbaspirillum* Root189 LPS and its corresponding *O*-deacylated form at 1.0 mg·mL-1. Dynamic Light Scattering (DLS) measurements revealed a single distribution centered at a hydrodynamic radius of 21.0 ± 1.0 nm (in red), necessary condition to evaluate, via Static Light Scattering (SLS), a proper molecular weight around 420 ± 20 KDa attributed to small aggregates consisting of around 15 units (LPS mw estimated around 10KDa) and with a radius of 21 nm. **(B)** Neutron reflectivity profiles (points) with model data fits (solid lines) for a DPPC (inner leaflet): *Herbaspirillum*-LPS (outer leaflet). The total SLD profile is shown on central panel. Shaded areas represent 95% confidence intervals determined by Bayesian error estimation. Volume fraction occupancy of the molecular moieties across the entire interface; silicon (black), silicon dioxide (grey); inner head groups (green); PC tails (red); LPS tails (purple); core/outer head group (Mid-Green), O-antigen (dark green), solution (blue).

3.4 Immunological studies.

Herbaspirillum Root189 LPS immune modulation in the host plant, including molecular determinants of recognition and impact of *O*-acetylation on the immunogenic potential, were then evaluated. To this aim, *Herbaspirillum* Root189 LPS as well as the *O*-deacylated polymer were evaluated for their ability to elicit the early immune responses such as apoplastic reactive oxygen species (ROS) production and cytosolic calcium influx in *Arabidopsis thaliana*, (Figure 5). While elicitation with native LPS did not induce ROS production, removal of its OPS-associated acyl groups inverted this behavior, leading to the detection of a substantial oxidative burst (Figure 5A). Measurements of cytosolic calcium influx, a second read-out for the rapid onset of immune responses, further confirmed this trend (Figure 5B). With the aim of evaluating microbial glycome interaction with host plant, *Herbaspirillum* Root189 LPS was

printed onto microarray slides at different concentrations and the binding of a panel of 35 lectins with diverse carbohydrate-binding specificities (Table S1) was examined. Meaningful binding signals were observed for a limited number of lectins (Figure 5C), namely *Hippeastrum hybrid* lectin (HHL), *Narcissus pseudonarcissus* lectin (NPL), *Galanthus nivalis* agglutinin (GNA), and, with lower intensity, concanavalin A (ConA), all known to recognize mannose-containing structures. For these lectins, LPS dose-dependent responses were detected.

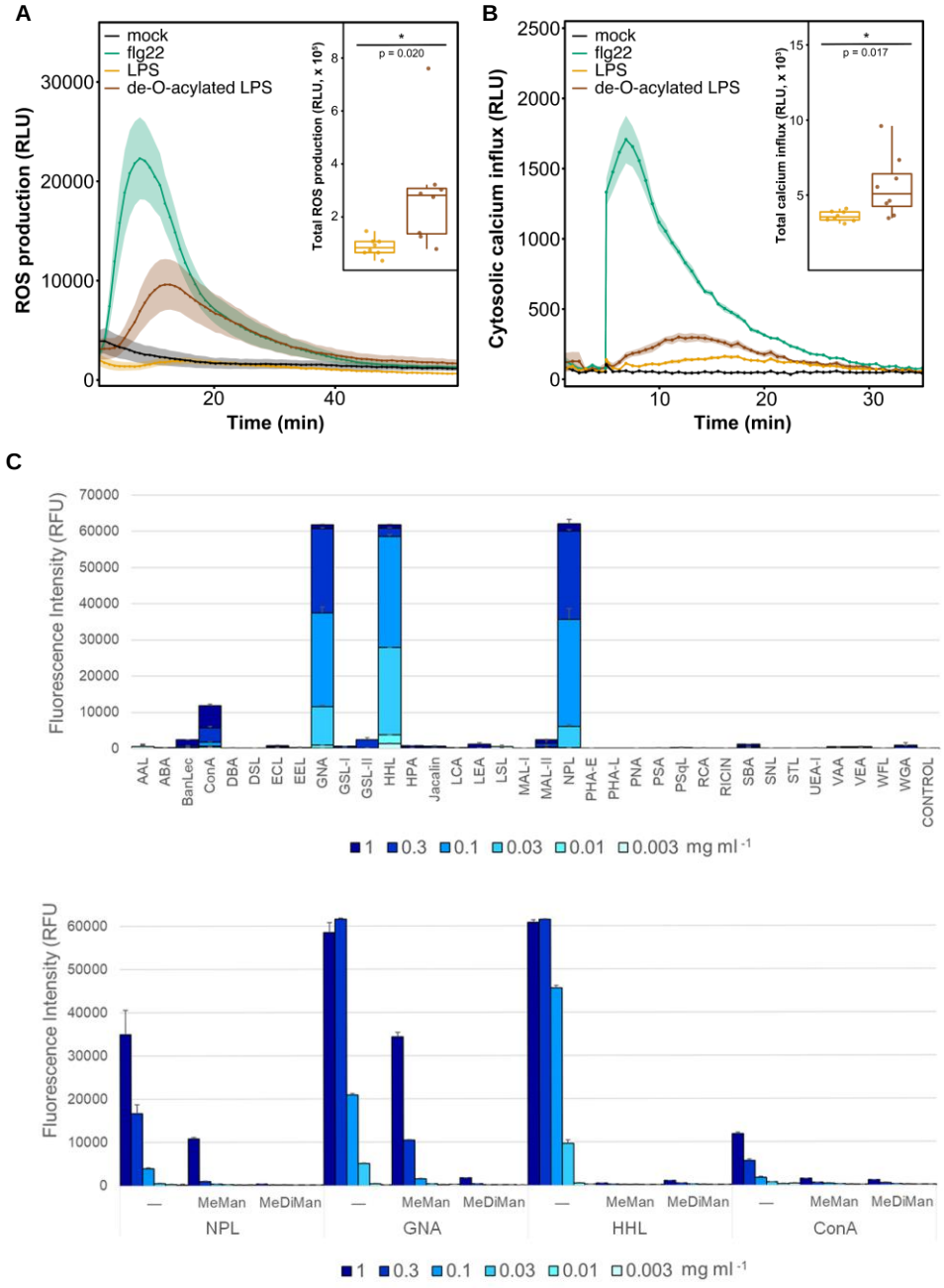

Figure 5. (A-B) Native *O*-acylation pattern protects *Herbaspirillum* LPS from activation of plant immune responses in *A. thaliana*. Activation of immunity in *A. thaliana* was measured upon treatment with sterile Milli-Q water (mock), 250 nM flg22, 200 µg ml-1 purified *Herbaspirillum* Root189 LPS and de-*O*-acylated LPS. **(A)** Luminol-based oxidative burst assays were performed with leaves of 28-days-old seedlings leaf discs. Each treatment is represented by eight leaf discs from different plants. ROS intensity is depicted as relative photon count (relative light units, RLU). **(B)** Changes in cytosolic calcium concentration were monitored using eight 13-days-old seedlings per treatment. Measured intensities of each well were normalized according to maximal

calcium levels after discharge of remaining aequorin with an EtOH/$CaCl_2$ solution. Values represent means±SEM. The inlets compare the total immune response activation (cumulative RLU intensities over time) of native and de-O-acylated *Herbaspirillum* LPS. Statistical significance was determined using two-tailed Welch's t-test (*: p-value ≤ 0.05). **(C)** Top: Screening of lectin binding to microarray-printed *Herbaspirillum* Root189 LPS. The LPS was printed as triplicates at six different concentrations (from 1 to 0.003 mg ml^{-1}), and the binding of a panel of biotin-labelled lectins was assayed, using AF647-streptavidin for detection. As control, one pad was incubated with buffer alone, followed by AF647-streptavidin. Bottom: Competition assays of lectin binding to microarray-printed *Herbaspirillum* Root189 LPS. The LPS was printed as triplicates at 1 to 0.003 mg ml^{-1}), and the binding of the lectins was assayed in the absence (-) or presence of 50 mM Methyl-α-D-mannopyranoside (MeMan) or 20 mM methyl-3-O-α-D-mannopyranosyl-α-D-mannopyranoside (MeDiMan).

Moreover, the binding was efficiently inhibited in the presence of methyl-α-D-mannose and/or methyl-α-(1-3)-D-mannose disaccharide in solution (Figures 5c), proving carbohydrate-mediated binding. On the other hand, no binding was detected for lectins exhibiting specificity for galactose, N-acetyl-galactosamine, fucose, or sialic acid. Of note, binding was equally not detected for other mannose-specific lectins tested, *e.g. Pisum sativum* (PSA), *Lens culinaris* (LCA) or *Vicia ervilia* (VEA) agglutinins (Figure 5C, Table S4), hinting at a singular arrangement of the LPS epitope recognized by HHL, NPL, GNA and ConA. Additionally, the restricted lectin-binding pattern observed in the microarray assays was further suggestive of the peculiar structure of the LPS O-antigen.

These findings clearly indicate that the acyl-substitution of *Herbaspirillum* OPS plays a pivotal role in evading plant immunity. Instead, these OPS glycan chemical modifications might instead trigger and switch a selective recognition by other proteins, *e.g.* lectins, tuned by acetylation/de-acetylation of the OPS chain. In this particular case, the D-Rha binding ability could be deemed of biological significance and be taken as further element of recognition by the plant right receptor.

4. Discussion

Plant-associated microbial community accounts for tens of thousands species and is referred to as the second genome of the plant (Berendsen, 2012). Plant microbiota, exactly as gut microbiota in mammals, is crucial for plant health poses a remarkable question: how does the plant innate immune system, which recognizes and actively defends against the proliferation of diverse pathogens, tolerate beneficial microbes or microbial commensal/symbiont communities? LPSs play a central role in plant-microbiota crosstalk, since they mediate plant-bacteria communication, protect from host environments, promote virulence but simultaneously betray bacteria to the host immune system (Ranf, 2016). We here examine a single example and demonstrate how the core root microbiota member *Herbaspirillum* Root189 expresses structurally tuned LPS to define its outer membrane properties and face host recognition, and also identify the features that impede its immune recognition.

The chemical composition of the LPSs from a number of diazotrophic nitrogen-fixing bacteria belonging to the genus *Herbaspirillum* have been studied, (Serrato, 2014) and a few LPS structure of *Herbaspirillum* species has been elucidated yet. In particular, the OPS from H. seropedicae Z78 consists of a glycerol-1-phosphate backbone partially substituted by N-acetyl-D-glucosamine (Velichko, 2018). More recently, a colitose-containing O-specific polysaccharide from the LPS of *Herbaspirillum frisingense* GSF30T has been reported (Velichko, 2018). We here report for the first time that *Herbaspirillum* Root189 LPS consists of a D-rhamnose based polysaccharide chain [-2)-Rha*p*-α–(1-3)-Rha*p*-β–(1-4)-Rha*p*-α-(1-3)-Rha*p*-α-(1-]$_n$, *O*-methylated and largely (but non-stoichiometrically) acetylated on the different rhamnose units. The main repeating unit exhibits a high grade of hydrophobicity with only one free hydroxyl group per sugar residue.

Our multidisciplinary approach has highlighted how LPS modifications with *O*-methyl and *O*-acetyl groups affect the immunological properties because of the biophysical properties. The OPS adopts an extended shape when de-acetylated, while higher conformational flexibility and a coiled like structuring is observed in the "natural" *O*-acetylated polymer. A moderate packed LPS bilayer, rather than a typical compact organization, is detected when organized in an asymmetric membrane-like structure, with a large spacing of glycolipid chains. Interestingly, the OPS is almost entirely covered on one side by *O*-methyl and *O*-acetyl substituents, leaving only one hydroxyl group per monosaccharide, thus tuning the ability of the sugar chain to interact with other polymers and/or receptor proteins and significantly changing its biophysical properties.

Furthermore, we found that the structural features of the LPS from *Herbaspirillum* Root189 can severely affect the interaction with the host plant. The hydrophobic interface as well as the huge substitution pattern likely drives and justifies the restricted lectin-binding pattern with only three mannose-binding lectins, namely, HHL, NPL, and GNA, giving strong binding signals in the microarray assays. These three lectins belong to a structurally conserved family of monocot mannose-binding lectins (MMBL) for which insecticidal activities, particularly against aphids, have been reported. (Ghequire, 2012) Interestingly, the bactericidal activity of *Pseudomonas* spp bacteriocins has been linked to the ability of the MMBL domain to recognize D-Rha units of LPS *O*-antigen (McCaughey, 2014). Therefore, considering the evolutionary relationships of *Pseudomonas* bacteriocins with those binding *Herbaspirillum* LPS, it is reasonable to presume that these lectins are also able to recognize D-Rha, as also highlighted by preliminary competition assays.

Interestingly, the extended *O*-acetyl substitution of the glycan chain indeed acts as a shielding strategy of the bacterial envelope to the plant immune system. This allows *Herbaspirillum* LPS to evade host recognition, by masking the cell-surface MAMPs to the plant. Considering that the LPS is involved in the very early recognition steps, we can deem the chemical decoration of *Herbaspirillum* Root189 LPS like a pass to successful colonization and beneficial and mutual interaction with the host plant.

Analogously, a cell wall polysaccharide from *Rhizobium* is recognized by the EPR3 plant receptor protein (Kawaharada, 2015), which is able to distinguish between EPS variants and thus to act positively in response to compatible or negatively in response to incompatible EPS. Likewise, *Arabidopsis* responses to *Herbaspirillum* LPS includes acetylated O-antigen recognition as a nonpathogenic signal, followed by the subsequent downregulation of defense-related immune responses. This is in agreement with the particular role and the peculiar chemistry of LPS in rhizobia where it serves to dampen the immune response and contribute establishment of a successful symbiosis (Sigida 2016; Silipo, 2011; Turska-Szewczuk, 2009; Di Lorenzo, 2020). However, a shielding strategy based on LPS chemistry can be used by pathogen bacteria to tune and revert their immune recognition. Indeed, the plant pathogen *X. fastidiosa* produces a high molecular weight L-rhamnose-rich O-antigen that mediate the surface attachment, aggregation, and biofilm maturation and delays immune recognition in grapevine (Clifford, 2013; Rapicavoli, 2018). This has interesting parallels with what happens on animal side where pathogens show host glycan structures in their LPS to pass unrecognized the innate immunity check.

5. Conclusions

Microbiota seems to sit at any crossroads of eukaryote world and influences the functionality of different organs of plants and mammals. In this latter, the LPS involvement in the host-gut microbiota cross-talk is receiving growing interest in its crucial structure-dependent role in triggering or preventing inflammation by modulating the host immune responses (Di Lorenzo, 2020). In plants, evasion or suppression of the plant immune system is not only crucial for pathogens to successfully infect plant hosts but also critical for commensals to colonize different plant niches. However, the cellular mechanisms and the microbial signals underlying host-microbiota interactions are still enigmatic. The sophisticated, yet unknown, immune mechanisms of the plant rhizosphere allow differentiating commensal and beneficial microbes from pathogens, indispensable to establish advantageous interactions for plant health. (Zhang, 2020) We have herein demonstrated that LPS from *Herbaspirillum*, a plant root microbe, when acetylated, acts as a chemical representative of a harmless microbe and therefore not raising any response. As recently shown, it is very likely that plant uses different lectin receptors to activate immune response or symbiosis process upon chemical recognition. We suggest that this process can also be adjuvated by microbial side in which the same glycan from the cell wall can be "decorated" to be specifically recognized for symbiosis.

Understanding the fundaments of interaction between distantly related plants and their host microbes will provide economic and environmental benefits, help genetic, biotech and engineering approaches

aimed at achieving resistance against pathogens, improving nutrient uptake, nitrogen fixation, for efficient use in sustainable agriculture.

Supplementary Materials

DLS and SLS discussion, Figure S1-S6 and table S1-S4

Acknowledgements

This study was supported by PRIN 2017 "Glytunes" (2017XZ2ZBK, 2019-2022) to AS; by the European Research Council (ERC) under the European Union's Horizon 2020 research and innovation programme under grant agreement No 851356 to RM. Neutron Reflectivity (NR) measurements were performed at the INTER instrument at ISIS Pulsed Neutron and Muon Source, Science and Technology Facilities Council, Rutherford Appleton Laboratory, Didcot, UK. The authors thank the ISIS facility for provision of beam time. MACR and DS gratefully acknowledge financial support from the Spanish Ministry of Science, Innovation, and Universities (RTI2018-099985-B-I00), and the CIBER of Respiratory Diseases (CIBERES), an initiative from the Spanish Institute of Health Carlos III (ISCIII). AZ and LM acknowledge support from the DFG (German Research Foundation) ZU 263/11-1.

Author Contributions

AS conceived the study, wrote the manuscript. AS and RM designed the research. All the authors contributed to execute the research, to analyse the data and to write the manuscript.

Competing interests:

The authors declare no competing financial interests

References

Bai, Y., Müller, D.B., Srinivas, G., Garrido-Oter, R., Potthoff, E., Rott, M., Dombrowski, N., Münch, P.C., Spaepen, S., Remus-Emsermann, M., Hüttel, B., McHardy, A.C., Vorholt, J.A., Schulze-Lefert, P. Functional overlap of the Arabidopsis leaf and root microbiota (2015). Nature 528(7582), 364-9.

Balsanelli, E., Serrato, R.V., de Baura, V.A., Sassaki, G., Yates, M.G., Rigo, L.U., Pedrosa, F.O., de Souza, E.M., Monteiro, R.A., (2012). *Herbaspirillum seropedicae* rfbB and rfbC genes are required for maize colonization Environ Microbiol 12, 2233–2244

Belin, B.J., Busset, N., Giraud, E., Molinaro, A., Silipo, A., Newman, D.K. Hopanoid lipids: from membranes to plant-bacteria interactions (2018). Nat Rev Microbiol. 16, 304–315.

Berendsen, R.L., Pieterse, C.M., Bakker, P.A. (2012). The rhizosphere microbiome and plant health, Trends Plant Sci. 17(8), 478-86,

Bligh E.G., Dyer W.J., A rapid method of total lipid extraction and purification, (1959). Can. J. Biochem. Phys. 37 911-917

Campanero-Rhodes MA, Childs RA, Kiso M, Komba S, Le Narvor C, Warren J, Otto D, Crocker PR, Feizi T. Biochem Biophys Res Commun. Carbohydrate microarrays reveal sulphation as a modulator of siglec binding (2006). 344(4):1141-6

Campanero-Rhodes MA, Kalograiaki I, Euba B, Llobet E, Ardá A, Jiménez-Barbero J, Garmendia J, Solís D. Exploration of Galectin Ligands Displayed on Gram-Negative Respiratory Bacterial Pathogens with Different Cell Surface Architectures (2021). Biomolecules, 11, 595

Ciucanu I., Kerek F., A simple and rapid method for the permethylation of carbohydrates, (1984) Carbohyd. Res. 131 209–217.

Clifford, J.C., Rapicavoli, J.N., Roper, M.C., A rhamnose-rich O-antigen mediates adhesion, virulence, and host colonization for the xylem-limited phytopathogen Xylella fastidiosa (2013). Mol Plant Microbe Interact. 26(6), 676-85.

Clifton, L.A., Skoda, M.W., Daulton, E.L., Hughes, A.V., Le Brun, A.P., Lakey, J.H., Holt, S.A. Asymmetric phospholipid: lipopolysaccharide bilayers, a Gram-negative bacterial outer membrane mimic, (2013). J. R. Soc Interface 10(89), 20130810,

De Castro C., Parrilli M., Holst O., Molinaro A., Microbe-associated molecular patterns in innate immunity: extraction and chemical analysis of gram-negative bacterial lipopolysaccharides, (2010). Methods Enzymol. 480 89-115

De La Torre-Ruiz, N., Ruiz-Valdiviezo, V.M., Rincón-Molina, C.I., Rodríguez-Mendiola, M., Arias-Castro, C., Gutiérrez-Miceli, F.A., Palomeque-Dominguez, H., Rincón-Rosales, R. Effect of plant growth-promoting bacteria on the growth and fructan production of Agave americana L (2016). Braz J Microbiol. 47(3), 587–596

Delaux, P.M., Schornack, S., Plant evolution driven by interactions with symbiotic and pathogenic microbes, (2021). Science 371, eaba6605

Di Lorenzo, F., Duda, K.A., Lanzetta, R., Silipo, A., De Castro, C., Molinaro, A. A Journey from Structure to Function of Bacterial Lipopolysaccharides. (2021). Chem Rev. doi: 10.1021/acs.chemrev.0c01321

Di Lorenzo, F., Pither, M.D., Martufi, M., Scarinci, I., Guzmán-Caldentey, J., Łakomiec, E., Jachymek, W., Bruijns, S.C.M., Santamaría, S.M., Frick, J.S., van Kooyk, Y., Chiodo, F., Silipo, A., Bernardini, M.L., Molinaro, A. Pairing Bacteroides vulgatus LPS Structure with Its Immunomodulatory Effects on Human Cellular Models (2020). ACS Cent Sci., 6(9), 1602-1616.

Di Lorenzo, F., Speciale, I., Silipo, A., Alías-Villegas, C., Acosta-Jurado, S., Rodríguez-Carvajal, M.Á., Dardanelli, M.S., Palmigiano, A., Garozzo, D., Ruiz-Sainz, J.E., Molinaro, A., Vinardell, J.M. Structure of the unusual Sinorhizobium fredii HH103 lipopolysaccharide and its role in symbiosis (2020). J Biol Chem. 295(32), 10969-10987

Erbs, G., Silipo, A., Aslam, S., De Castro, C., Liparoti, V., Flagiello, A., Pucci, P., Lanzetta, R., Parrilli, M., Molinaro, A., Newman, M.A., Cooper, R.M. Peptidoglycan and muropeptides from pathogens Agrobacterium and Xanthomonas elicit plant innate immunity: structure and activity (2008). Chem. Biol. 15, 438-448

Ghequire, MGK, Loris, R., De Mot, R., MMBL proteins: from lectin to bacteriocin Biochemical Society Transactions (2012). 40, 1553–9

Hacquard, S., Spaepen, S., Garrido-Oter, R., Schulze-Lefert, P. Interplay Between Innate Immunity and the Plant Microbiota (2017). Annu. Rev. Phytopathol. 55, 565–89

Hayafune, M., Berisio, R., Marchetti, R., Silipo, A., Kayama, M., Desaki, Y., Arima, S., Squeglia, F., Ruggiero, A., Tokuyasu, K., Molinaro, A., Kaku, H., Shibuya, N. Chitin-induced activation of immune signaling by the rice receptor CEBiP relies on a unique sandwich-type dimerization (2014). PNAS 111, E404-E413

Kawaharada, Y., Kelly, S., Nielsen, M.W., Hjuler, C.T., Gysel, K., Muszyński, A., Carlson, R.W., Thygesen, M.B., Sandal, N., Asmussen, M.H., Vinther, M., Andersen, S.U., Krusell, L., Thirup, S., Jensen, K.J., Ronson, C.W., Blaise, M., Radutoiu, S., Stougaard, J. Receptor-mediated exopolysaccharide perception controls bacterial infection (2015). Nature 523(7560), 308-12

Laezza, A., Casillo, A., Cosconati, S., Biggs, C. I., Fabozzi, A., Paduano, L., Iadonisi, A., Novellino, E., Gibson, M. I., Randazzo, A., Corsaro. M. M., Bedini, E. Decoration of Chondroitin Polysaccharide with Threonine: Synthesis, Conformational Study, and Ice-Recrystallization Inhibition Activity. Biomacromolecules (2017). 18, 2267–76

Lomakin, A., Teplow, D. B., Benedek, G. B., Quasielastic light scattering for protein assembly studies. (2005). Methods Mol. Biol. 299, 153-74

Marchetti, R., Forgione, R.E., Fabregat, F.N., Di Carluccio, C., Molinaro, A., Silipo, A. Solving the structural puzzle of bacterial glycome (2021). Curr Opin Struct Biol. 68, 74-83

McCaughey, L.C., Grinter, R., Josts, I., Roszak, A.W., Waløen, K.I., Cogdell, R.J., Milner, J., Evans, T., Kelly, S., Tucker, N.P., Byron, O., Smith, B., Walker, D. Lectin-like bacteriocins from Pseudomonas spp. utilise D-rhamnose containing lipopolysaccharide as a cellular receptor (2014). PLOS Pathogens 10, e1003898,

Monteiro, R.A., Balsanelli, E., Wassem, R., Marin, A.M., Brusamarello-Santos, L.C.C., Schmidt, M.A., Tadra-Sfeir, M.Z., Pankievicz, V.C.S., Cruz, L.M., Chubatsu, L.S., Pedrosa, F.O., Souza, E.M. Herbaspirillum-plant interactions: Microscopical, histological and molecular aspects (2012). Plant Soil 356, 175–196

Nicolardi, S., Joseph, A.A., Zhu, Q., Shen, Z., Pardo-Vargas, A., Chiodo, F., Molinaro, A., Silipo, A., van der Burgt, Y.E.M., Yu, B., Seeberger, P.H., Wuhrer, M., Analysis of Synthetic Monodisperse Polysaccharides by Wide Mass Range Ultrahigh-Resolution MALDI Mass Spectrometry (2021). Anal Chem. 93(10), 4666-4675,

Paduano, L. Sartorio R., Vitagliano, V., Albright, J. G., Miller, D. G. Measurement of the mutual diffusion coefficients at one composition of the four-component system α-cyclodextrin-L-phenylalanine-monobutylurea-H2O at 25 °C. (1992). J. Phys. Chem.96, 7478–83

Perfetti, M., Gallucci, N., Russo-Krauss, I., Radulescu, A., Pasini, S., Holderer, O., D'Errico, G., Vitiello, G., Bianchetti, G.O., Paduano, L. Revealing the Aggregation Mechanism, Structure, and Internal Dynamics of Poly(vinyl alcohol) Microgel Prepared through Liquid–Liquid Phase Separation, (2020). Macromolecules 53(3), 852–861

Ranf, S. Immune Sensing of Lipopolysaccharide in Plants and Animals: Same but Different (2016). PLoS Pathog. 12(6), e1005596

Rapicavoli, J.N., Blanco-Ulate, B., Muszyński, A., Figueroa-Balderas, R., Morales-Cruz, A., Azadi, P., Dobruchowska, J.M., Castro, C., Cantu, D., Roper, M.C. Lipopolysaccharide O-antigen delays plant innate immune recognition of Xylella fastidiosa (2018). Nat. Commun. 9(1), 390,

Roe D.R., Cheatham T. E., PTRAJ and CPPTRAJ: Software for Processing and Analysis of Molecular Dynamics Trajectory Data (2013). J. Chem. Theory Comput., 9 (7). 3084-3095

Serrato, R.V., Lipopolysaccharides in diazotrophic bacteria (2014). *Front. Cell. Infect. Microbiol.* 4, 119, 1-6

Schlemper, T.R., Dimitrov, M.R., Silva Gutierrez, F.A.O., van Veen, J.A., Silveira, A.P.D., Kuramae, E.E. Effect of Burkholderia tropica and Herbaspirillum frisingense strains on sorghum growth is plant genotype dependent (2018). PeerJ. 6, e5346

Sigida, E.N., Fedonenko, Y.P., Shashkov, A.S., Arbatsky, N.P., Zdorovenko, E.L., Konnova, S.A., Ignatov, V.V., Knirel, Y.A., (2016). Elucidation of a masked repeating structure of the O-specific polysaccharide of the halotolerant soil bacteria Azospirillum halopraeferens Au4 Beilstein J. Org. Chem. 12, 636–642

Silipo, A., Leone, M.R., Erbs, G., Lanzetta, R., Parrilli, M., Chang,W.S., Newman, M.A., Molinaro, A. A unique bicyclic monosaccharide from the Bradyrhizobium lipopolysaccharide and its role in the molecular interaction with plants, (2011). Angew. Chemie 50 (52), 12610-12612

Tadra-Sfeir, M.Z., Souza, E.M., Faoro, H., Müller-Santos, M., Baura, V.A., Tuleski, T.R., Rigo, L.U., Yates, M.G., Wassem, R., Pedrosa, F.O., Monteiro, R.A., Naringenin regulates expression of genes involved in cell wall synthesis in Herbaspirillum seropedicae (2011). Appl Environ Microbiol 77, 2180–2183

Trivedi, P., Leach, J.E., Tringe, S.G., Sa, T., Singh, BK, Plant-microbiome interactions: from community assembly to plant health, (2020). Nat. Rev. Microbiol.18, 607–621

Turska-Szewczuk, A., Lotocka, B., Kutkowska, J., Król, J., Urbanik-Sypniewska, T., Russa, R. The incomplete substitution of lipopolysaccharide with O-chain prevents the establishment of effective symbiosis between Mesorhizobium loti NZP2213.1 and Lotus corniculatus (2009). Microbiol Res 164(2), 163-73.

Velichko, N.S., Surkina, A.K., Fedonenko, Y.P., Zdorovenko, E. L., Konnova, S.A. Structural Peculiarities and Biological Properties of the Lipopolysaccharide from *Herbaspirillum seropedicae* Z78 (2018). *Microbiology* **87,** 635–641.

Velichko NS, Kokoulin MS, Sigida EN, Kuchur PD, Komissarov AS, Kovtunov EA, Fedonenko YP. (2020). Int J Biol Macromol. 161, 891-897.

Vaccaro, M., Mangiapia, G., Paduano, L., Gianolio, E., Accardo, A., Tesauro, D., Morelli, G. Structural and Relaxometric Characterization of Peptide Aggregates Containing Gadolinium Complexes as Potential Selective Contrast Agents in MRI. (2007). Chem. Phys. Chem., 8(17), 2526–2538.

Vitiello G., Luchini A., D'Errico G., Santamaria R.,Capuozzo A., Irace C. , Daniela Montesarchio D., and Paduano L. Cationic liposomes as efficient nanocarriers for the drug delivery of an anticancer cholesterol-based ruthenium complex, (2015). J. Mater. Chem. B, 3, 3011-3023

Vitiello, G., Oliva, R., Petraccone, L., Vecchio, P.D., Heenan, R.K., Molinaro, A., Silipo, A., D'Errico, G., Paduano, L. Covalently bonded hopanoid-Lipid A from Bradyrhizobium: The role of unusual molecular structure and calcium ions in regulating the lipid bilayers organization (2021). Colloid Interface Sci. 594, 891-901

Wanke, A., Malisic, M., Wawra, S., Zuccaro, A. Unraveling the sugar code: the role of microbial extracellular glycans in plant-microbe interactions (2021). Journal of Experimental Botany, 72(1), 15–35

Wanke, A., Rovenich, H., Schwanke, F., Velte, S., Becker, S., Hehemann, J.H., Wawra, S., Zuccaro, A. Plant species-specific recognition of long and short β-1,3-linked glucans is mediated by different receptor systems (2020). Plant J. 102(6), 1142-1156

Westphal O., Jann K.. Bacterial lipopolysaccharides. Extraction with phenol water and further applications of the procedure. in: R.L. Whistler (Eds.), Methods in Carbohydrate Chemistry, Academic, New York, NY, 1965, pp. 83–91.

Zhang, C., He, J., Dai, H., Wang, G., Zhang, X., Wang, C., Shi, J., Chen, X., Wang, D., Wang, E. Discriminating symbiosis and immunity signals by receptor competition in rice (2021). PNAS 118(16), e2023738118

Zhang, J., Coaker, G., Zhou, J.M., Dong, X. Plant Immune Mechanisms: From Reductionistic to Holistic Points of View (2020) Mol Plant. 13(10), 1358-137